Water Science and Engineering 2020, 13(4): 307−316

HOSTED BY

ELSEVIER

Available online at www.sciencedirect.com

Water Science and Engineering

journal homepage: wse.hhu.edu.cn

Batch and fixed-bed column studies of selenite removal from contaminated water by orange peel-based sorbent

Bárbara Pérez Mora [a,b], Fernando A. Bertoni [a,b], María F. Mangiameli [a,b], Juan C. González [a,b], Sebastián E. Bellú [a,b,*]

[a] *Faculty of Biochemical and Pharmaceutical Sciences, National University of Rosario, Rosario S2002LRK, Argentina*
[b] *Chemistry Institute of Rosario, National Council of Scientific and Technological Research, Rosario S2002LRK, Argentina*

Received 28 February 2020; accepted 26 October 2020
Available online 11 December 2020

Abstract

Orange peel is a biomass derived from citrus processing with desirable properties for metal sorption. In recent years, orange peel has been used to remove various heavy metals and toxic oxyanions. Selenium (Se) is an essential trace element for mammals. However, when the concentration of selenium exceeds an umbral limit, it becomes toxic. In this study, orange peel was used to treat Se(IV)-contaminated water. A high sorption capacity of 32.5 mg/g was obtained at a temperature of 20°C and a pH of 2.0. Hydroxyl groups bound Se(IV) to the surface of the orange peel. The sorption process was spontaneous and endothermic. A chemical sorption mechanism was involved in the removal of Se(IV). The Thomas and modified dose-response models were used to simulate the experimental breakthrough curves. The bed depth service time model was used to calculate the critical bed depth (Z_0), and the calculated Z_0 value was 1.6 cm. This study reveals that orange peel is a useful sorbent for Se(IV), and can be used for the purification of Se(IV)-contaminated water.

Keywords: Sorption; Orange peel; Removal of heavy metal; Selenium-contaminated water; Sorbent; Breakthrough curve

1. Introduction

Orange peels are a byproduct of citrus processing, and they have desirable properties for metal sorption (Lugo-Lugo et al., 2012). Orange is the most popular and consumed fruit in Argentina. The production of oranges in Argentina is approximately 900 000 t per year. Half of the production is destined for the local market as fresh fruit. The rest is used for juice production and exportation. Approximately 75% of orange fruit becomes a byproduct or waste after juice extraction. This produced byproduct, to some extent, can be utilized as a metal sorbent in the process of water remediation.

Recently, orange peel has been used to remove various heavy metals and toxic oxyanions, such as copper(II) (Romero-Cano et al., 2016; Guiza, 2017), chromium(III) (Lugo-Lugo et al., 2012), chromium(VI) (Olea-Mejía et al., 2017), iron(III) (Lugo-Lugo et al., 2012), cadmium(II) (Kelly-Vargas et al., 2012; Trana et al., 2016), lead(II) (Kelly-Vargas et al., 2012; Abdelhafez and Li, 2016), arsenic(V), and arsenic(III) (Biswas et al., 2008). Previous studies demonstrate the desirable properties of this biomaterial for the sorption of heavy metals and toxic oxyanions.

Selenium (Se) is an essential trace element for mammals. However, when the selenium concentration reaches an umbral limit, it becomes toxic (Xiao et al., 2016). Selenium appears in

This work was supported by the National Agency of Scientific and Technological Promotion (Grant No. PICT 2016-1611), the Santa Fe Province Agency of Science, Technology and Innovation (Grant No. AC 2015-0005), and National University of Rosario (Grant No. BIO517).
* Corresponding author.
E-mail addresses: bellu@iquir-conicet.gov.ar, sbellu@fbioyf.unr.edu.ar (Sebastián E. Bellú).
Peer review under responsibility of Hohai University.

https://doi.org/10.1016/j.wse.2020.12.003

the environment in inorganic and organic forms. Anthropogenic contamination with selenium occurs because of the use of selenium-containing insecticides and herbicides. In addition, coal-based industries, mining, and the oil industry generate selenium pollution to the environment (Miller and Goodman, 1996).

The inorganic forms of selenium are the most toxic selenium species (Latorre et al., 2013). Their observed effects include skin diseases, damage to cardiovascular and respiratory systems, neurological disorders, and cancer (Mondal et al., 2006). The harmful effects of selenium are increased by biomagnification in aquatic organisms (Adio et al., 2017). According to the Environmental Protection Agency, USA, the mass fraction of selenium in drinking water should be less than 0.05×10^{-6}. In effluents, its mass fraction ranges from 0.1×10^{-6} to 20×10^{-6}. The high levels of selenium imply that these effluents must be treated before discharge (Awual et al., 2015).

Many techniques have been used to remediate selenium-contaminated water, including sorption (Dobrowolski and Otto, 2013), ion exchange (Nishimura et al., 2007), electrocoagulation membrane processing (Mavrov et al., 2006), and biological treatments (Zhang and Frankenberger Jr., 2003). Of these techniques, sorption is the simplest and cheapest approach, and sorbents can be regenerated and reused in many cycles. A variety of sorbents have been employed, including activated carbon (Dobrowolski and Otto, 2013), chitosan-clay composites (Bleiman and Mishael 2010), iron and aluminum oxides (Su et al., 2008), modified sand (Kuan et al., 1998), magnetic nanocomposites (Lu et al., 2017), and ion-imprinted polymers (Mafu et al., 2016).

Sorption reduction processes have attracted more attentions for their potential use in the treatment of high-valent metal ions (Alharbi et al., 2020). Carbon nitride-based nanomaterials have been successfully applied in the treatment of water contaminated by arsenic(V) and uranium(VI) (Wang et al., 2020). Biochar-based materials have received special attention for their potential use in the sorption of high-valent metal ions, such as chromium(VI), arsenic(V), and selenium(IV) (Hu et al., 2020).

However, some sorbents currently used have a low sorption capacity and cannot easily be separated from solutions. As a result, it is necessary to develop new sorbents with a high sorption capacity and high separation efficiency. This study applied orange peel biomass as a sorbent of selenite ions in batch and continuous systems and investigated the efficacy of orange peel in removal of SeO_3^{2-} from naturally contaminated groundwater. Additionally, the benefits of employment of this system in the purification of real water samples in fixed-bed columns were verified.

2. Materials and methods

In this study, all chemicals were of analytical reagent grade and used without further purification. Certain amounts of Na_2SeO_3 (Sigma-Aldrich, 99% purity) were dissolved in Milli-Q water (resistivity of 18 MΩ·cm) to obtain Se(IV) solutions.

2.1. Orange peel sorbent preparation

Orange peel was obtained from oranges harvested near the city of Rosario (Argentina). The orange peel bio-sorbent was flushed out with Milli-Q water, dehydrated at 40°C for 24 h, and then pulverized and sifted (particle size: 2−3 mm). As described in Bertoni et al. (2015) and Blanes et al. (2016), the pH value at the point of zero charge (pH_z) was estimated.

2.2. Statistical experimental design

To recognize the main factors that have significant influence on the sorption capacity of orange peel for SeO_3^{2-}, an experimental screening was carried out. According to the Plackett-Burman design (Bruns et al., 2006), several factors were selected, including the contact time (t = 20−60 min), temperature (T = 20−60°C), sorbent mass (m = 0.01−0.50 g), pH (pH = 1−6), initial SeO_3^{2-} concentration (ρ_0 = 173 mg/L), and batch volume (10.0 mL). In addition, optimization of the variable response was performed after experimental screening. The optimized response was achieved through the central composite design method (Bezerra et al., 2008). The obtained regression model was validated with the analysis of variance (ANOVA) method. The mathematical functions were resolved, and statistical tests were conducted using the Design Expert V7.0 software.

2.3. Batch sorption experiments

Suspensions with a known amount of orange peel mass and solutions with different Se(IV) concentrations were prepared. The biomass mass was (0.15 ± 0.02) g at a pH of 2.0. The quantitative measurements of SeO_3^{2-} were spectrophotometrically conducted at 540 nm by employing 2-hydroxy-1-napthaldehyde-orthoaminophenol in dimethylformamide (Ahmed et al., 2015). Standard stock solutions were analyzed in triplicate, and the estimated analytical data reproducibility was within 5%.

The kinetic and thermodynamic sorption processes were studied at 20°C, 30°C, and 40°C. Selenite uptake by orange peel biomass was calculated as follows:

$$q = \frac{(\rho_0 - \rho)V}{m} \tag{1}$$

where q is the sorption capacity, which is the ratio of the mass of sorbed SeO_3^{2-} to that of orange peel (mg/g); ρ is the effluent SeO_3^{2-} concentration (mg/L); m is the amount of orange peel (g); and V is the batch volume (L).

In this study, scanning electron microscopy (SEM, Fei QUANTA 200F) was used to analyze the surface structure of the orange peel, and electron dispersive spectroscopy (EDS, EDAX) with a Si/Li detector was employed to detect the sorbed selenium at the biomass surface. Each measurement was conducted in low vacuum mode (chamber pressure:

20−40 Pa) with an operational distance of 10−12 mm. Images were collected on non-coated samples at a high voltage (HV) of 15 kV under low vacuum conditions, and semi-quantitative EDS analysis of the amount of sorbed selenium was conducted. The EDS and SEM analyses were carried out at the Technological and Scientific Center of Rosario.

To identify orange peel functional groups and Se(IV)-loaded biomass, Fourier transformed infrared (FTIR) spectroscopy (PerkinElmer) was adopted. Data from infrared (IR) absorbances were obtained at the wave number of 400−4 000 cm^{-1} by employing KBr pellets.

Specific surface areas and porosities of orange peel sorbents were determined with the Micrometrics ASAP 2020 V4.02 automatic analyzer based on N_2 sorption-desorption isotherms.

2.4. Fixed-bed column studies

Polypropylene columns with an internal diameter of 1.4 cm and length of 15 cm were filled with different amounts of orange peel, which were used in the continuous selenite ion sorption processes. The package density was kept constant, and sorbents were packed into the columns to a desired height under the action of gravity. The selenite solution of 140 mg/L at room temperature with a pH of 2.0 was pumped through the columns with an ascending flow of 1.0 mL/min. At different time intervals, the effluent Se(IV) concentration was measured for each 1.0-mL sample. The sorption capacity of orange peel for selenite ions was determined as follows:

$$q=\frac{\rho_0 Q}{1\,000m}\int_0^t\left(1-\frac{\rho}{\rho_0}\right)\mathrm{d}t \tag{2}$$

where t is the contact time (min), and Q is the volumetric flow (mL/min).

It is feasible to derive a breakthrough curve from a plot of ρ/ρ_0 against time to describe the column bed performance. Given an effluent with ρ of 0.05 mg/L, the breakthrough time t_b (min) was defined as $\rho/\rho_0 = 0.05$. When ρ/ρ_0 was equal to 0.95, the saturation time t_{sat} (min) was fixed.

2.5. Analysis of real contaminated water

Groundwater in Santa Fe Province of Argentina was examined with standard methods (Clesceri and GrenbergEaton, 1998). The following water characteristics were investigated: calcium (475.8 mg/L), phosphate (0.520 mg/L), nitrite (0.068 mg/L), ammonia (8.45 μg/L), nitrate (45.6 mg/L), sulphate (1 109.5 mg/L), organic matter (2.54 mg/L), total arsenic (0.064 5 mg/L), molybdenum(VI) (less than 0.001 mg/L), selenium(IV) (0.205 mg/L), pH (7.80), and the total hardness (1 802.5). The sorption process for groundwater treatment was carried out in a continuous mode by employing a 9-cm bed height with an upward flow rate of 1.0 mL/min.

It is possible to minimize the operational costs of sorption processes if the sorbent can be reused in several cycles of sorption-desorption. Therefore, it is necessary to study the continuous process of desorption. With this methodology, contaminants were concentrated in a smaller volume, as compared with the starting volume. Desorption experiments were conducted under the following conditions: an upward flow of 1.0 mL/min and a 0.10 mol/L NaOH solution used as the eluent reagent. The desorption efficiency was determined for two successive cycles of sorption-desorption, expressed as follows:

$$E_d=\frac{n_r}{n_s}\times 100\% \tag{3}$$

where E_d is the desorption efficiency (%), and n_r and n_s are the released and sorbed selenium (mol), respectively.

3. Results and discussion

3.1. Removal process optimization

The Plackett-Burman design was used to analyze experimental data. All the studied factors (pH, time, and biomass dose) were significant with a p-value less than 0.05, and pH was shown to have the strongest effect.

To optimize and enhance the selenium removal process, the central composite design method was developed. Multiple regression analysis was used to test experimental data. Eq. (4) describes the removal efficiency of SeO_3^{2-} by orange peel, as a function of pH, sorbent mass, and contact time:

$$E_f=116.49-26.07\alpha-106.59m+0.43t-221.61m^2+22.93\alpha m-0.87mt \tag{4}$$

where E_f is the removal efficiency of SeO_3^{2-} by orange peel, and α is the pH value. Table 1 shows the ANOVA results of the response surface quadratic model, where DF, SE, SSE, and MSE refer to the degree of freedom, standard error, sum of squared errors, and mean squared error, respectively. An F-value of 41.69 was obtained with a low p-value, indicating that the regression model is highly significant. With a high coefficient of determination ($R^2 = 0.961\,6$), the model is suitable for simulating the Se(VI) sorption process. Based on Eq. (4), the efficiencies of selenite removal with different orange peel doses, pH values, and time periods were predicted. The highest SeO_3^{2-} removal efficiency was achieved at 120 min with an orange peel dose of 15.0 g/L and a pH of 2.0. At this pH value, it was found that $HSeO_3^-$ and H_2SeO_3 were the major Se(IV) species when the HYDRA and MEDUSA programs were employed (http://www.kemi.kth.se/medusa).

Fig. 1 shows the variation of ΔpH against the initial pH value, where ΔpH is the difference between the initial and equilibrium pH values (after 24-h contact time). The pH_z value was determined to be 3.5 with ΔpH = 0, indicating that the orange peel surface with pH values lower than 3.5 was positively charged and could attract hydrogenselenite anions. The E_f value of Se(IV) removal obtained under the optimum experimental conditions was 86.5%, which was in

Table 1
Estimated regression coefficients and ANOVA results for response surface quadratic model.

Term	Regression coefficient	DF	SE	SSE	MSE	*F*-value	*p*-value
E_f	116.49	6	2.34	12 618.79	2 103.13	41.69	<0.000 1
α	−26.07	1	1.92	10 653.00	10 653.00	211.15	<0.000 1
m	−106.59	1	1.92	309.87	309.87	6.14	0.032 6
t	0.43		1.92	465.76	465.76	9.23	0.012 5
m^2	−221.61	1	1.97	600.11	600.11	11.89	0.006 2
αm	22.93		2.51	289.80	289.80	5.74	0.037 5
mt	−0.87		2.51	300.25	300.25	5.95	5.950 0
Residual		10		504.53	50.45		
Error		2		0.027	0.013		
Lack of fit		8		504.50	63.06	1.56	0.067 2

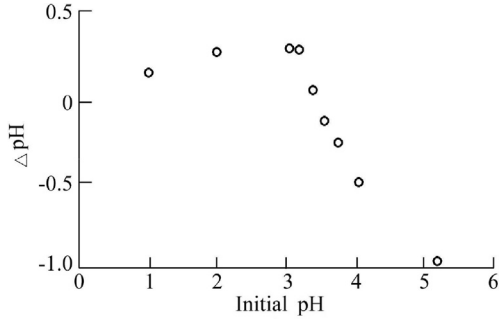

Fig. 1. Determination of pH_z of orange peel (m = 0.15 g, and T = 20°C).

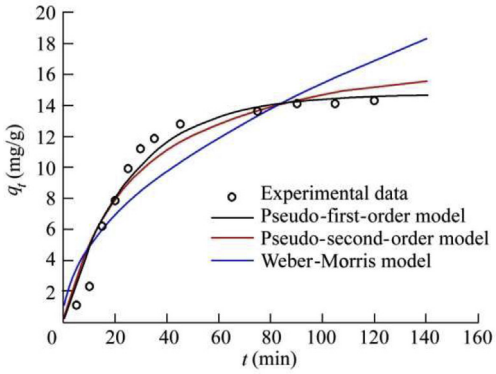

Fig. 2. Observed sorption rate fitted by pseudo-first-order and pseudo-second-order kinetic models and Weber-Morris diffusion model (m = 0.15 g, T = 20°C, pH = 2.0, and ρ_0 = 173 mg/L).

concordance with the theoretical value of 86.2% estimated by Eq. (4).

3.2. Sorption rate

The sorption rate is important because it provides information for subsequent design of continuous bed sorption systems (Hawari et al., 2009). In this study, the pseudo-first-order and pseudo-second-order kinetic models were adopted to describe the sorption mechanism against time. The pseudo-first-order kinetic model is expressed as follows:

$$q_t = q_e\left(1 - e^{-k_1 t}\right) \tag{5}$$

where k_1 is the first-order-rate constant (min^{-1}); and q_e and q_t are the q values at equilibrium and time t (mg/g), respectively. The pseudo-second-order kinetic model is expressed as follows:

$$q_t = \frac{t}{1/\left(k_2 q_e^2\right) + t/q_e} \tag{6}$$

where k_2 is the second-order-rate constant (g/(mg·min)) (Ho and McKay, 1999).

Fig. 2 demonstrates the observed sorption rate at 20°C, fitted by the pseudo-first-order and pseudo-second-order kinetic models. This figure and Table 2 indicate that the experimental results were better fitted by the pseudo-first-order kinetic model. Moreover, theoretical values of q_e obtained from the pseudo-first-order kinetic model agreed with the experimental values.

Most sorption processes can take place through different and complex mechanisms (Bertoni et al., 2015). To verify whether the rate-limiting step was related to an intraparticle diffusion process, the Weber-Morris diffusion model was used, which is expressed as follows:

$$q_t = k_{id} t^{1/2} \tag{7}$$

where k_{id} is the intraparticle diffusion rate constant. As shown in Fig. 2, the removal process did not follow the Weber-Morris diffusion model. This implies that the rate-limiting step involved both the bindig of sorbate to the active surface and intraparticle diffusion (Bertoni et al., 2015).

The activation energy parameter (E_a) was obtained through linearization of the Arrhenius plot. An E_a value that does not exceed 4.184 kJ/mol implies a physical sorption mechanism, while an E_a value greater than 8.4 kJ/mol implies a chemisorption process. In this study, the E_a value was 96.5 kJ/mol, indicating a chemisorption process.

3.3. Isotherm

Surface properties and affinity of a sorbent can be characterized by sorption isotherm models. The simplest and most commonly used models to describe the experimental equilibrium data are the Langmuir, Freundlich, and Dubinin-Radushkevich isotherms. The non-linear Langmuir isotherm model is expressed as follows (Langmuir, 1918):

Table 2
Characteristic parameters of different models and R^2 (m = 0.15 g, pH = 2.0, and ρ_0 = 173 mg/L).

T (°C)	Pseudo-first-order model			Pseudo-second-order model			Weber-Morris diffusion model	
	q_e (mg/g)	k_1 (10^{-2} min^{-1})	R^2	q_e (mg/g)	k_2 (10^{-3} g/(mg·min))	R^2	k_{id} (g/(mg·min$^{1/2}$))	R^2
20	8.9 ± 0.1	1.67 ± 0.05	0.998 5	13.0 ± 0.4	0.95 ± 0.05	0.997 8	0.64 ± 0.02	0.957 5
30	4.6 ± 0.3	5.3 ± 0.7	0.980 8	6.4 ± 0.6	7.0 ± 0.8	0.977 0	0.68 ± 0.02	0.951 6
40	3.3 ± 0.1	21 ± 2	0.986 5	4.3 ± 0.3	45 ± 8	0.968 1	0.82 ± 0.05	0.886 2

$$q_e = \frac{q_m K_L \rho_e}{1 + K_L \rho_e} \tag{8}$$

where ρ_e is the SeO_3^{2-} concentration at equilibrium (mg/L), q_m is the maximum amount of selenite ions sorbed by per gram of biomass (mg/g), and K_L is the Langmuir equilibrium constant. The separation factor (R_L) can be used to determine whether the Langmuir model is properly used:

$$R_L = \frac{1}{1 + K_L c_h} \tag{9}$$

where c_h is the highest SeO_3^{2-} concentration (mol/L). An R_L value between 0 and 1 suggests a favorable sorption process. The Freundlich isotherm model (Freundlich, 1907) is as follows:

$$q_e = K_F \rho_e^{1/n} \tag{10}$$

where K_F is the Freundlich equilibrium constant, and $1/n$ is the coefficient of heterogeneity. To determine whether the Langmuir or Freundlich model was suitable for modeling experimental data, the Sips isotherm model (Sips, 1948) was also used in this study, which is expressed as follows:

$$q_e = \frac{q_m b_s \rho_e^N}{1 + b_s \rho_e^N} \tag{11}$$

where N is the Sips exponent, and b_s is the Sips constant. The Dubinin-Radushkevich (D-R) isotherm model (Rand, 1975) can be obtained as follows:

$$q_e = q_m e^{-\beta \varepsilon^2} \tag{12}$$

where β is a constant (mol^2/J^2), and ε is the Polanyi potential. The free energy of sorption can be estimated with the constant β, which is expressed as follows:

$$E = \frac{1}{(2\beta)^{1/2}} \tag{13}$$

where E is the free energy of sorption (J/mol). Table 3 presents the numerical values of E and other constants in different isotherm models. The obtained E values ranged from 8.5 kJ/mol to 14.4 kJ/mol, indicating that Se(IV) sorption onto orange peel occurred through a chemisorption mechanism (Bertoni et al., 2015). At the temperatures under study, the Langmuir model fitted experimental data quite well. R_L values implied that the sorption mechanism developed favorably. The Sips exponent at different temperatures had a value close to $N = 1$. Therefore, it is feasible to use the Langmuir isotherm model for this sorption system.

The isotherm profiles of selenite sorption at three temperature values are shown in Fig. 3. The experimental results are well represented by the Langmuir isotherm model at the three studied temperatures. Table 4 compares the sorption capacity of orange peel with those of other materials as sorbents for selenite, and orange peel shows a higher sorption capacity than other sorbents. Considering the cheap value of this biomass, it could be a better choice as a useful selenite removal sorbent.

3.4. Thermodynamics

In industrial processes, it is necessary to know whether a certain sorption process is spontaneous or not. For this reason, the thermodynamic parameters were investigated in this study. The change of Gibbs free energy (ΔG) is estimated with the formula produced by Chen et al. (2011), which is expressed as follows:

$$\Delta G = RT \ln(c_w K_L) \tag{14}$$

Table 3
Characteristic parameters of different isotherm models and R^2 (m = 0.15 g, pH = 2.0, t = 3.0 h, and ρ_0 = 0.10–700.00 mg/L).

T (°C)	Langmuir isotherm model				Freundlich isotherm model		
	q_m (mg/g)	k_L (10^{-2} L/mg)	R_L	R^2	k_F	$1/n$	R^2
20	32.5 ± 0.4	0.40 ± 0.05	0.714	0.992 2	0.8 ± 0.3	0.53 ± 0.06	0.957 2
30	7.6 ± 0.4	1.0 ± 0.2	0.500	0.989 3	0.4 ± 0.1	0.49 ± 0.05	0.965 4
40	5.1 ± 0.4	1.8 ± 0.3	0.357	0.976 5	0.4 ± 0.2	0.39 ± 0.08	0.997 5

T (°C)	Sips isotherm model				D-R isotherm model			
	q_m (mg/g)	b (10^{-2})	N	R^2	q_m (mg/g)	β (10^9 mol^2/J^2)	E (10^3 J/mol)	R^2
20	30.8 ± 0.3	0.13 ± 0.07	1.3 ± 0.1	0.996 6	50 ± 3	5 ± 1	10.7 ± 0.7	0.921 1
30	7.5 ± 0.3	1.2 ± 0.6	1.1 ± 0.2	0.989 6	10.2 ± 0.7	7 ± 2	8.5 ± 0.5	0.911 3
40	4.8 ± 0.3	0.45 ± 0.07	1.2 ± 0.2	0.990 4	6.7 ± 0.5	2.4 ± 0.6	14.4 ± 0.8	0.778 9

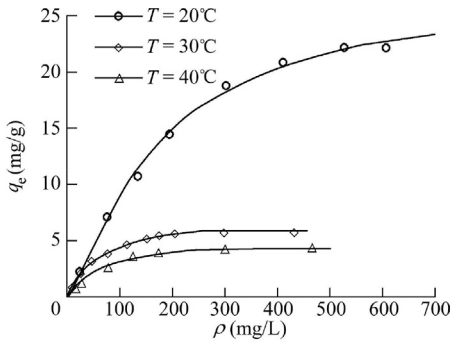

Fig. 3. Sorption isotherms obtained by Langmuir isotherm model (m = 0.15 g, pH = 2.0, t = 3.0 h, and ρ_0 = 0.10−700.00 mg/L).

Table 4
Comparison of sorption capacities of orange peel for Se(IV) and other sorbents reported in literature.

Sorbent	Se(IV) sorption capacity (mg/g)	Reference
Amido amine-graphene	60.90	Xiao et al. (2016)
Al(III)/SiO_2	32.70	Chan et al. (2009)
Fe_3O_4-chitosan	15.62	Seyed Dorraji et al. (2017)
Fe−C	2.50	Zhang et al. (2008)
Green seaweed	0.50	Filotea et al. (2017)
Hydroxyapatite	5.51	Kongsri et al. (2013)
Chitosan	1.35	Kongsri et al. (2013)
Nano-TiO_2	8.46	Zhang et al. (2009)
Orange peel	32.50	This study

where c_w is the water molarity, with c_w = 55.5 mol/L; and R is the universal gas constant. The changes in enthalpy (ΔH) and entropy (ΔS) were estimated by Eq. (15) (Chen et al., 2011):

$$\ln(c_w K_L) = \frac{\Delta S}{R} - \frac{\Delta H}{RT} \tag{15}$$

A positive ΔS value of 282.0 J/(K·mol) was obtained in this study, suggesting an increase in the randomness of the system. Furthermore, a positive ΔH value of 57.5 kJ/mol was obtained, revealing the endothermic nature of the sorption process. This behavior was previously described in Liu and Liu (2008). A negative ΔG value of −24.98 kJ/mol obtained in this study indicates that the sorption process was spontaneous.

3.5. Isosteric heat of sorption

It is necessary to know the thermodynamic parameters for the designed removal processes (Unnithan and Anirudhan, 2001; Sircar, 2005). In this study, the Clausius-Clapeyron equation was used to calculate the isosteric heat of sorption, which can be calculated with Eq. (16):

$$\frac{\mathrm{d}\ln \rho_e}{\mathrm{d}T} = -\frac{\Delta H_{st}}{RT^2} \tag{16}$$

where ΔH_{st} is the isosteric heat of sorption (kJ/mol). Fig. 4 shows the plots of ln ρ_e versus T^{-1} at different q values, and ΔH_{st} was obtained by calculating the slope of these plots.

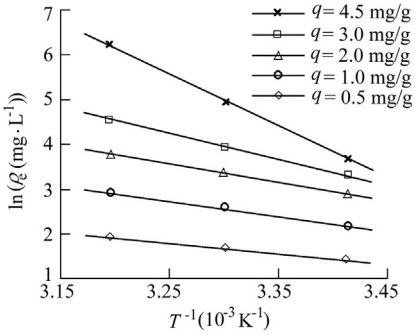

Fig. 4. Plots of ln ρ_e against T^{-1} for sorption of SeO_3^{2-} ions onto orange peel at different q levels.

Fig. 5 shows ΔH_{st} increasing with q. This behavior reveals that orange peel has an energetically homogeneous surface. Similar results have been reported by Blanes et al. (2016).

3.6. Result of FTIR analysis

Fig. 6 demonstrates the FTIR spectra of orange peels. The observed numerous signals indicate the complex composition of the biomass. Table 5 shows the major stretching vibrations of orange peel and SeO_3^{2-}-loaded orange peel. After selenite sorption by the orange peel, some variations could be detected in the FTIR spectra. Symmetric and antisymmetric stretching vibrations corresponding to SeO_3^{2-} appeared (with wave numbers of 817 cm^{-1} and 776 cm^{-1}, respectively) (Frost et al., 2014). The signals assigned to O−H (3 520 cm^{-1}) and C−O (1 095 cm^{-1}) stretching vibrations were shifted (Blanes et al., 2016). No changes in antisymmetric and symmetric stretching vibrations of C=O were observed. This evidence confirms that only hydroxyl groups were involved in binding selenite ions onto the surface of the orange peel.

3.7. Analysis of orange peel surface

SEM images were obtained to investigate the orange peel surface. Fig. 7(a) and (b) displays the surface structure of the original orange peel. This biomass presented a rough surface with high porosity. After selenite sorption, smothering occurred at the surface of the orange peel (Fig. 7(c) and (d). Orange peel is predominantly constituted by cellulose, and pectin is the principal component of this biomass extracellular

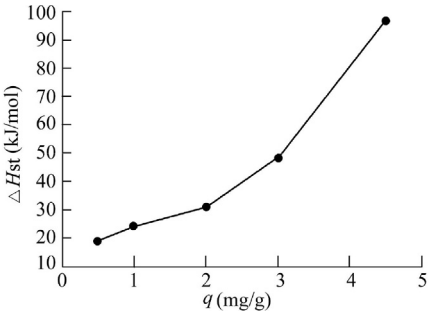

Fig. 5. Variation of isosteric heat of sorption with surface loading of SeO_3^{2-} ions onto orange peel.

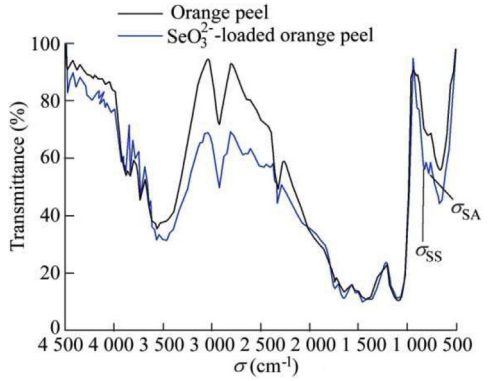

Fig. 6. FTIR spectra of orange peel and SeO_3^{2-}-loaded orange peel.

Table 5
Characteristic IR signals of orange peel and SeO_3^{2-}-loaded orange peel.

Sample	IR signal (cm^{-1})					
	σ_{OH}	σ_{CO}	σ_{COA}	σ_{COS}	σ_{SA}	σ_{SS}
Orange peel	3 520	1 095	1 643	1 447		
SeO_3^{2-}-loaded orange peel	3 475	1 076	1 643	1 447	776	817

Note: σ_{OH} and σ_{CO} are the wave numbers of O−H and C−O streching vibrations, respectively; σ_{COA} and σ_{COS} are the wave numbers of antisymmetric and symmetric stretching vibrations of C=O, respectively; and σ_{SA} and σ_{SS} are the wave numbers of antisymmetric and symmetric stretching vibrations corresponding to SeO_3^{2-}, respectively.

matrix (Bizzani et al., 2017). These biopolymers present active sites that could be available to bind Se(IV) and allow selenite anion sorption, resulting in the modification of surface morphology. These changes cause smothering of the structures on orange peel sorbents.

The EDS analysis of orange peel after selenite sorption was carried out at an HV of 15 kV, and it displayed a signal corresponding to selenite at 1.4 keV. This study confirmed that selenium was attached to the orange peel surface. The BET surface area of orange peel particles was 2.9 m^2/mg, the total pore volume was 0.854 cm^3/mg, and the pore size was 1 175 nm. These results confirmed the existence of micropores in the particle structure.

3.8. Selenite removal mechanism

Knowledge of the oxyanion sorption mechanism allows for improvement of experimental conditions for toxic anion removal by biomass. Many possible sorption mechanisms have been proposed, one of which is the sorbate binding onto active surface groups in biomass (Bertoni et al., 2015; Blanes et al., 2016; Carnevale et al., 2017). Sorption parameters of activation energy and mean free energy support the chemisorption mechanism. Because pectin is the major biopolymer at the surface of orange peel, binding of selenite anions to this polysaccharide was proposed.

The highest selenite ion removal efficiency was achieved at a pH of 2.0. At this pH value, $HSeO_3^-$ ions were attracted and stabilized by the orange peel surface with $pH_z = 3.5$. At higher pH values, OH^- competed with selenite ions for surface sorption sites, and repulsion between the negatively-charged orange peel surface and selenite ions occurred as well.

In order to confirm whether electrostatic stabilization occurred, an ionic strength effect experiment was conducted. This experiment demonstrated that an increment of ionic strength produced a negative effect in sorption of selenite ions at a pH of 2. Nevertheless, some sorption was observed at high ionic strength. This confirms that electrostatic interaction is not the only sorption mechanism.

This study indicated that selenite ions are attracted and stabilized by the sorbent surface, and hydroxyl groups at the orange peel surface act as active sites for chemisorption. In addition, based on the IR results, hydroxyl functional groups were considered the active sites, involved in binding selenite anions. This sorption mechanism combining electrostatic interaction and chemical bonding of ions to the sorbent surface agrees with the findings of Bertoni et al. (2018).

3.9. Sorption dynamics in fixed-bed columns

Mathematical models can be used to analyze the sorption dynamics in fixed-bed columns. To investigate breakthrough curve behaviors and changes under different operational conditions, the Thomas and modified dose-response models (Thomas, 1944; Yan et al., 2001) were used in this study. The Thomas model is expressed as follows:

$$\frac{\rho}{\rho_0} = \frac{1}{1 + \exp[(q_{Th}m - \rho_0 vt)k_{Th}/v]} \tag{17}$$

where k_{Th} is the Thomas rate constant (L/(mg·min)), v is the flow rate of the effluent (L/min), and q_{Th} is the theoretical

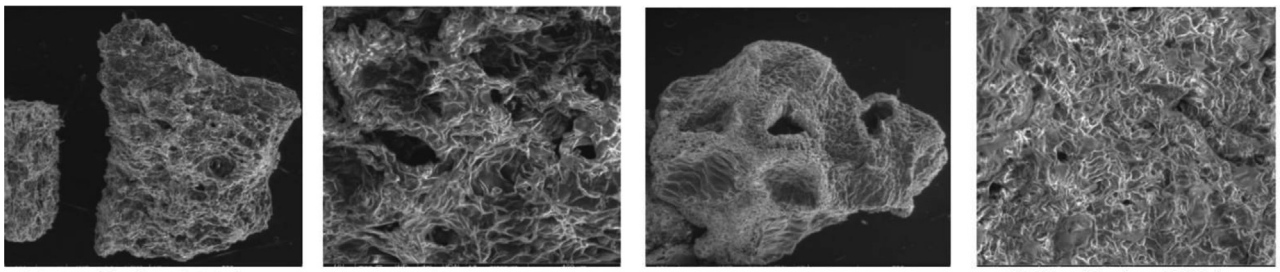

(a) Magnification of 220 times before Se(IV) sorption
(b) Magnification of 800 times before Se(IV) sorption
(c) Magnification of 165 times after Se(IV) sorption
(d) Magnification of 800 times after Se(IV) sorption

Fig. 7. Orange peel SEM images at HV of 15 kV.

saturated sorption capacity (mg/g). The modified dose-response model is described as follows:

$$\frac{\rho}{\rho_0}=1-\frac{1}{1+(vt/b)^a} \tag{18}$$

where a and b are the parameters.

Fig. 8 displays the breakthrough curves at bed heights of 3.0 cm, 6.0 cm, and 9.0 cm, respectively. This figure indicates that the modified dose-response model best fit experimental data. Table 6 exhibits the experimental values of the breakthrough and saturation time, as well as the selenite ion uptake. Table 7 shows the coefficients of determination (R^2) and parameters of both mathematical models. Fig. 8 and Tables 6 and 7 were obtained under the following experimental conditions: ρ_0 = 140.0 mg/L, v = 1.0 mL/min, T = 20°C, and pH = 2.0. As shown in Tables 6 and 7, the simulated q_{Th} values were close to the experimental results (q_{obs}). As the bed height rose, k_{Th} decreased, revealing that the kinetic process slowed down with the increase of the column length. This behavior was previously mentioned in other studies (Bertoni et al., 2015; Carnevale et al., 2017). R^2 values of the modified dose-response model ranged from 0.992 2 to 0.997 9, demonstrating a strong correlation between the experimental and theoretical values.

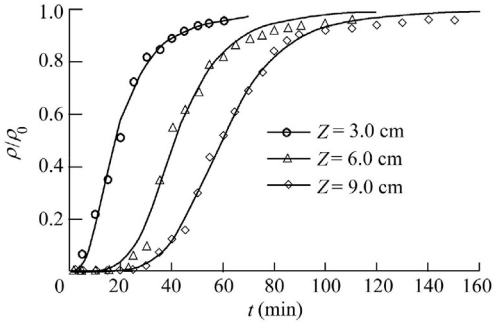

Fig. 8. Breakthrough curves obtained from modified dose-response model at different bed heights.

Table 6
Experimental parameters of breakthrough curves.

Bed height (cm)	Experimental parameter			
	t_b (min)	t_{50} (min)	t_{sat} (min)	q_{obs} (mg/g)
3.0	6	20	55	3.08 ± 0.08
6.0	20	41	100	3.31 ± 0.07
9.0	33	59	130	3.37 ± 0.05

Note: t_{50} is the time as ρ/ρ_0 = 0.5.

The increase of bed height resulted in the rise of the parameter b. This result agrees with the findings of previous studies (Bertoni et al., 2015; Carnevale et al., 2017).

To perform the scale-up investigation, the bed depth service time (BDST) model was applied (Bohart and Adams, 1920). The mathematical expression in linear form that relates the operation time to the bed depth (Z) can be expressed as follows:

$$t=\frac{N_0}{\rho_0 v}Z-\frac{1}{k_{BDST}\rho_0}\ln\left(\frac{\rho_0}{\rho}-1\right) \tag{19}$$

where k_{BDST} is the kinetic constant (L/(mg·min)), and N_0 is the volumetric sorption capacity (mg/L).

In a fixed-bed column at four different ρ/ρ_0 values, the iso-concentration straight lines for Se(IV) sorption were evaluated (Fig. 9). At a low breakthrough state (lower ρ/ρ_0 value), N_0 values were smaller in comparison with the whole biomass bed sorption capacity (Bohart and Adams, 1920) because some active sites remained free. Moreover, an excellent correlation was established by examination of the breakthrough curve at ρ/ρ_0 of 50%, where the logarithmic term was zero. This result confirms that it is feasible to use the BDST model to simulate the selenite ion removal process with orange peel sorbent.

The critical bed depth (Z_0) is the minimum theoretical bed height that produces an effluent concentration lower than the breakthrough concentration at the initial moment. Z_0 can be estimated by Eq. (20):

$$Z_0=\frac{v}{k_{BDST}N_0}\ln\left(\frac{\rho_0}{\rho_b}-1\right) \tag{20}$$

where ρ_b is the effluent concentration at the breakthrough time. For the orange peel sorbent, Z_0 was equal to 1.6 cm.

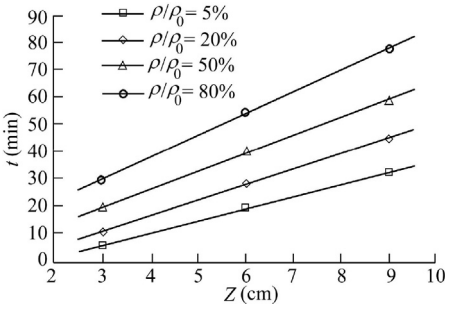

Fig. 9. Results of BDST model in different breakthrough states with different ρ/ρ_0 values (ρ_0 = 140.0 mg/L, v = 1.0 mL/min, T = 20°C, and pH = 2.0).

Table 7
Parameters for Thomas and modified dose-response models.

Bed height (cm)	Thomas model				Modified dose-response model			
	k_{Th} (10^4 L/(mg·min))	q_{Th} (mg/g)	R^2	χ^2	a	b (10^4)	R^2	χ^2
3.0	10.0 ± 1.0	2.8 ± 0.1	0.984 5	0.002 01	2.6 ± 0.1	1.82 ± 0.04	0.995 4	0.000 92
6.0	8.0 ± 0.5	3.04 ± 0.06	0.979 3	0.002 84	4.4 ± 0.2	4.13 ± 0.06	0.992 2	0.000 93
9.0	6.0 ± 0.3	3.890 ± 0.003	0.993 2	0.002 33	5.0 ± 0.1	5.92 ± 0.04	0.997 9	0.000 81

Note: Small values of χ^2 demonstrate the consistency between modeled results and observations, based on the statistical hypothesis test.

3.10. Analysis of real samples

Finally, several tests were performed with orange peel as a bio-sorbent for selenite ions in the contaminated groundwater. Two sorption-desorption cycles were conducted to detect sorbent reusability. In the first cycle, the breakthrough time and treated water quantity were 33 min and 0.033 L, respectively. To evaluate desorption/recovery of selenite from the column, a 0.1 mol/L NaOH solution was used as the desorbent reagent. The volume of NaOH solution was 0.01 L in the first cycle, and the percentage of the observed selenite desorption was 70%. In the second cycle, the breakthrough time decreased to 15 min, losing over 55% of the sorption capacity. This deficiency in the selenite removal capacity was probably due to the partial desorption of selenium ions. The second sorption cycle began with some selenite ions strongly bound to the orange peel biomass. Therefore, a few active sites were blocked, causing a loss in contaminant removal. However, the water quality of effluent implies that the water treated with orange peel could be used for domestic purposes.

4. Conclusions

In this study, the feasibility of orange peel as a new sorbent of Se(IV) was validated. The FTIR analysis confirmed the contribution of hydroxyl groups to the binding of selenite anions at the orange peel surface. The chemical sorption mechanism was confirmed with kinetic and thermodynamic investigations. To analyze continuous sorption, experimental data were used to fit three kinetic models. The main conclusions can be summarized as follows:

(1) Orange peel demonstrates a higher sorption capacity than other sorbents that have previously been reported in the literature.

(2) Breakthrough curves were best fitted by the modified dose-response model, and the BDST model can be used to scale up the system.

(3) Orange peel-based sorbent could be an excellent alternative for removal of selenite ions from real groundwater samples, and this sorption system could be employed for household purposes.

(4) Two sorption-desorption cycles demonstrate that the column can be used in continuous sorption systems.

(5) Finally, the low cost, high availability, and high sorption capability of orange peel make this citric waste an effective sorbent for selenite ions present in groundwater and contaminated effluent.

Declaration of competing interest

The authors declare no conflicts of interest.

References

Abdelhafez, A.A., Li, J., 2016. Removal of Pb(II) from aqueous solution by using biochars derived from sugar cane bagasse and orange peel. J. Taiwan Inst. of Chem. Eng. 61, 367−375. https://doi.org/10.1016/j.jtice.2016.01.005.

Adio, S.O., Omar, M.H., Asif, M., Saleh, T.A., 2017. Arsenic and selenium removal from water using biosynthesized nanoscale zero-valent iron: A factorial design analysis. Process Saf. Environ. Protect. 107, 518−527. https://doi.org/10.1016/j.psep.2017.03.004.

Ahmed, M.J., Islam, M.T., Nime, M.J., 2015. A highly selective and sensitive spectrophotometric method for the determination of selenium using 2-hydroxy-1-napthaldehyde-orthoaminophenol. Anal. Methods 7(18), 7811−7823. https://doi.org/10.1039/C5AY01311A.

Alharbi, N.S., Hu, B., Hayat, T., Rabah, S.O., Alsaedi, A., Zhuang, L., Wang, X., 2020. Efficient elimination of environmental pollutants through sorption-reduction and photocatalytic degradation using nanomaterials. Front. Chem. Sci. Eng. 14, 1123−1135. https://doi.org/10.1007/s11705-020-1923-z.

Awual, R., Hasan, M., Khaleque, A., 2015. Efficient selenium(IV) detection and removal from water by tailor-made novel conjugate adsorbent. Sensor. Actuator. B Chem. 209, 194−202. https://doi.org/10.1016/j.snb.2014.11.010.

Bertoni, F.A., Medeot, A.C., González, J.C., Sala, L.F., Bellú, S.E., 2015. Application of green seaweed biomass for MoVI sorption from contaminated waters: Kinetic, thermodynamic and continuous sorption studies. J. Colloid Interface Sci. 446, 122−132. https://doi.org/10.1016/j.jcis.2015.01.033.

Bertoni, F.A., González, J.C., García, S., Sala, L.F., Bellú, S.E., 2018. Application of chitosan in removal of molybdate ions from contaminated water and groundwater. Carbohydr. Polym. 180, 55−62. https://doi.org/10.1016/j.carbpol.2017.10.027.

Bezerra, M.A., Santelli, R.E., Oliveira, E.P., Villar, L.S., Esclaleira, L.A., 2008. Response surface methodology (RSM) as a tool for optimization in analytical chemistry. Talanta 76(5), 965−977. https://doi.org/10.1016/j.talanta.2008.05.019.

Biswas, B.K., Inoue, J.I., Inoue, K., Ghimire, K.N., Harada, H., Ohto, K., Kawakita, H., 2008. Adsorptive removal of As(V) and As(III) from water by a Zr(IV)-loaded orange waste gel. J. Hazard Mater. 154(1−3), 1066−1074. https://doi.org/10.1016/j.jhazmat.2007.11.030.

Bizzani, M., Menezes Flores, D.W., Colnago, L.A., Ferreira, M.D., 2017. Non-invasive spectroscopic methods to estimate orange firmness, peel thickness, and total pectin content. Microchem. J. 133, 168−174. https://doi.org/10.1016/j.microc.2017.03.039.

Blanes, P.S., Bordoni, M.E., González, J.C., García, S.I., Atria, A.M., Sala, L.F., Bellú, S.E., 2016. Application of soy hull biomass in removal of Cr(VI) from contaminated waters: Kinetic, thermodynamic and continuous sorption studies. J. Environ. Chem. Engin. 4(1), 516−526. https://doi.org/10.1016/j.jece.2015.12.008.

Bleiman, N., Mishael, Y.G., 2010. Selenium removal from drinking water by adsorption to chitosan-clay composites and oxides: Batch and columns tests. J. Hazard Mater. 183(1−3), 590−595. https://doi.org/10.1016/j.jhazmat.2010.07.065.

Bohart, G.S., Adams, E.Q., 1920. Some aspects of the behavior of charcoal with respect to chlorine. J. Am. Chem. Soc. 42(3), 523−544. https://doi.org/10.1021/ja01448a018.

Bruns, R.E., Scarmino, I.S., de Barros Neto, B., 2006. Statistical Design: Chemometrics. Elsevier, Amsterdam.

Carnevale, B., Blanes, P., Sala, L.F., Bellú, S.E., 2017. Removal of molybdate anions from contaminated waters by brown algae biomass in batch and continuous processes. Chem. Technol. Biotechnol. 92(6), 1298−1305. https://doi.org/10.1002/jctb.5124.

Chan, Y.T., Kuan, W.H., Chen, T.Y., Wang, M.K., 2009. Adsorption mechanism of selenate and selenite on the binary oxide systems. Water Res. 43(17), 4412−4420. https://doi.org/10.1016/j.watres.2009.06.056.

Chen, S., Yue, Q., Gao, B., Li, Q., Xu, X., 2011. Removal of Cr(VI) from aqueous solution using modified corn stalks: Characteristic, equilibrium, kinetic and thermodynamic study. Chem. Eng. J. 168(2), 909−917. https://doi.org/10.1016/j.cej.2011.01.063.

Clesceri, L.S., Greenberg, A.E., Eaton, A.D., 1998. Standard Methods for the Examination of Water and Wastewater Analysis, 21st ed. APHA, Washington, D.C.

Dobrowolski, R., Otto, M., 2013. Preparation and evaluation of Fe-loaded activated carbon for enrichment of selenium for analytical and environmental purposes. Chemosphere 90(2), 683−690. https://doi.org/10.1016/j.chemosphere.2012.09.049.

Filotea, C., Ungureanu, G., Boaventura, R., Santos, S., Volf, I., Botelho, C., 2017. Green macroalgae from the Romanian coast of Black Sea: Physico-chemical characterization and future perspectives on their use as metal anions biosorbents. Process Saf. Environ. Protect. 108, 34−43. https://doi.org/10.1016/j.psep.2016.06.002.

Freundlich, H.M.F., 1907. Uber die adsorption in losungen. Z. Phys. Chem. 57, 385−470 (in German). https://doi.org/10.1515/zpch-1907-5723.

Frost, R.L., Cejka, J., Scholz, R., López, A., Theiss, F.L., Xi, Y., 2014. Vibrational spectroscopic study of the uranyl selenite mineral derriksite $Cu_4UO_2(SeO_3)_2(OH)_6\cdot H_2O$. Spectrochim. Acta Mol. Biomol. Spectrosc. 117, 473−477. https://doi.org/10.1016/j.saa.2013.08.026.

Guiza, S., 2017. Biosorption of heavy metal from aqueous solution using cellulosic waste orange peel. Ecol. Eng. 99, 134−140. https://doi.org/10.1016/j.ecoleng.2016.11.043.

Hawari, A., Rawajfih, Z., Nsour, N., 2009. Equilibrium and thermodynamic analysis of zinc ions adsorption by olive oil mill solid residues. J. Hazard Mater. 168(2−3), 1284−1289. https://doi.org/10.1016/j.jhazmat.2009.03.014.

Ho, Y.S., McKay, G., 1999. Pseudo-second order model for sorption processes. Process Biochem. 34(5), 451−465. https://doi.org/10.1016/S0032-9592(98)00112-5.

Hu, B., Ai, Y., Jin, J., Hayat, T., Alsaedi, A., Zhuang, L., Wang, X., 2020. Efficient elimination of organic and inorganic pollutants by biochar and biochar-based materials. Biochar 2, 47−64. https://doi.org/10.1007/s42773-020-00044-4.

Kelly-Vargas, K., Cerro-Lopez, M., Reyna-Tellez, S., Bandala, E.R., Sanchez-Salas, J.L., 2012. Biosorption of heavy metals in polluted water, using different waste fruit cortex. Phys. Chem. Earth 37−39, 26−29. https://doi.org/10.1016/j.pce.2011.03.006.

Kongsri, S., Janpradit, K., Buapa, K., Techawongstien, S., Chanthai, S., 2013. Nanocrystalline hydroxyapatite from fish scale waste: Preparation, characterization and application for selenium adsorption in aqueous solution. Chem. Eng. J. 215−216, 522−532. https://doi.org/10.1016/j.cej.2012.11.054.

Kuan, W.H., Lo, S.L., Wang, M.K., Lin, C.F., 1998. Removal of Se(IV) and Se(VI) from water by aluminum-oxide-coated sand. Water Res. 32(3), 915−923. https://doi.org/10.1016/S0043-1354(97)00228-5.

Langmuir, I., 1918. The adsorption of gases on plane surfaces of glass, mica and platinum. J. Am. Chem. Soc. 40(9), 1361−1403. https://doi.org/10.1021/ja02242a004.

Latorre, C.H., García, J.B., Martín, S.G., Crecente, R.M.P., 2013. Solid phase extraction for the speciation and preconcentration of inorganic selenium in water samples: Review. Anal. Chim. Acta 804, 37−49. https://doi.org/10.1016/j.aca.2013.09.054.

Liu, Y., Liu, Y.J., 2008. Biosorption isotherms, kinetics and thermodynamics. Separ. Purif. Technol. 61(3), 229−242. https://doi.org/10.1016/j.seppur.2007.10.002.

Lu, Z., Yu, J., Zeng, H., Liu, Q., 2017. Polyamine-modified magnetic graphene oxide nanocomposite for enhanced selenium removal. Separ. Purif. Technol. 183, 249−257. https://doi.org/10.1016/j.seppur.2017.04.010.

Lugo-Lugo, V., Barrera-Díaz, C., Ureña-Núñez, F., Bilyeu, B., Linares-Hernández, I., 2012. Biosorption of Cr(III) and Fe(III) in single and binary systems onto pretreated orange peel. J. Environ. Manag. 112, 120−127. https://doi.org/10.1016/j.jenvman.2012.07.009.

Mafu, L.D., Mamba, B.B., Msagati, T.A.M., 2016. Synthesis and characterization of ion imprinted polymeric adsorbents for the selective recognition and removal of arsenic and selenium in wastewater samples. J. Saudi Chem. Soc. 20(5), 594−605. https://doi.org/10.1016/j.jscs.2014.12.008.

Mavrov, V., Stamenov, S., Todorova, E., Chmiel, H., Erwe, T., 2006. New hybrid electrocoagulation membrane process for removing selenium from industrial wastewater. Desalination 201(1−3), 290−296. https://doi.org/10.1016/j.desal.2006.06.005.

Miller, T.M., Goodman, W.H., 1996. Removal of Selenium from Water by Complexation with Polymeric Dithiocarbamates. Nalco Chemical Company, Napervlue.

Mondal, P., Majumder, C.B., Mohanty, B., 2006. Laboratory based approaches for arsenic remediation from contaminated water: Recent developments. J. Hazard Mater. 137(1), 464−479. https://doi.org/10.1016/j.jhazmat.2006.02.023.

Nishimura, T., Hashimoto, H., Nakayama, M., 2007. Removal of selenium(VI) from aqueous solution with polyamine-type weakly basic ion exchange resin. Separ. Sci. Technol. 42(14), 3155−3167. https://doi.org/10.1080/01496390701513107.

Olea-Mejía, O., Cabral-Prieto, A., Salcedo-Castillo, U., López-Telleza, G., Olea-Cardoso, O., López-Castañares, R., 2017. Orange peel + nano-structured zero-valent-iron composite for the removal of hexavalent chromium in water. Appl. Surf. Sci. 423, 170−175. https://doi.org/10.1016/j.apsusc.2017.06.173.

Rand, B., 1975. On the empirical nature of the Dubinin-Radushkevich equation of adsorption. J. Colloid Interface Sci. 56(2), 337−346. https://doi.org/10.1016/0021-9797(76)90259-9.

Romero-Cano, L.A., Gonzalez-Gutierrez, L.V., Baldenegro-Perez, L.A., 2016. Biosorbents prepared from orange peels using instant controlled pressure drop for Cu(II) and phenol removal. Ind. Crop. Prod. 84, 344−349. https://doi.org/10.1016/j.indcrop.2016.02.027.

Seyed Dorraji, M.S., Amani-Ghadim, A.R., Hanifehpour, S., Woo Joo, S., Figoli, A., Carraro, M., Tasselli, F., 2017. Performance of chitosan based nanocomposite hollow fibers in the removal of selenium(IV) from water. Chem. Eng. Res. Des. 117, 309−317. https://doi.org/10.1016/j.cherd.2016.10.043.

Sips, R., 1948. On the structure of a catalyst surface. J. Chem. Phys. 16, 490−495. https://doi.org/10.1063/1.1746922.

Sircar, S., 2005. Heat of adsorption on heterogeneous adsorbents. Appl. Surf. Sci. 252(3), 647−653. https://doi.org/10.1016/j.apsusc.2005.02.082.

Su, T., Guan, X., Gu, G., Wang, J., 2008. Adsorption characteristics of As(V), Se(IV), and V(V) onto activated alumina: Effects of pH, surface loading, and ionic strength. J. Colloid Interface Sci. 326(2), 347−353. https://doi.org/10.1016/j.jcis.2008.07.026.

Thomas, H.C., 1944. Heterogeneous ion exchange in a flowing system. J. Am. Chem. Soc. 66, 1664−1666. https://doi.org/10.1021/ja01238a017.

Trana, H.N., You, S.J., Chao, H.P., 2016. Thermodynamic parameters of cadmium adsorption onto orange peel calculated from various methods: A comparison study. J. Environ. Chem. Engin. 4(3), 2671−2682. https://doi.org/10.1016/j.jece.2016.05.009.

Unnithan, M.R., Anirudhan, T.S., 2001. The kinetics and thermodynamics of sorption of chromium(VI) onto the iron(III) complex of a carboxylated polyacrylamide-grafted sawdust. Ind. Eng. Chem. Res. 40(12), 2693−2701. https://doi.org/10.1021/ie0009740.

Wang, X., Li, X., Wang, J., Zhu, H., 2020. Recent advances in carbon nitride-based nanomaterials for the removal of heavy metal ions from aqueous solution. J. Inorg. Mater. 35(3), 260−270. https://doi.org/10.15541/jim20190436.

Xiao, W., Yan, B., Zeng, H., Liu, Q., 2016. Dendrimer functionalized graphene oxide for selenium removal. Carbon 105, 655−664. https://doi.org/10.1016/j.carbon.2016.04.057.

Yan, G., Viraraghavan, Y., Chen, M., 2001. A new model for heavy metal removal in a biosorption column. Adsorpt. Sci. Technol. 19, 25−43. https://doi.org/10.1260/0263617011493953.

Zhang, L., Liu, N., Yang, L., Lin, Q., 2009. Sorption behavior of nano-TiO_2 for the removal of selenium ions from aqueous solution. J. Hazard Mater. 170(2−3), 1197−1203. https://doi.org/10.1016/j.jhazmat.2009.05.098.

Zhang, N., Lin, L.S., Gang, D., 2008. Adsorptive selenite removal from water using iron-coated GAC adsorbents. Water Res. 42(14), 3809−3816. https://doi.org/10.1016/j.watres.2008.07.025.

Zhang, Y., Frankenberger Jr., W.T., 2003. Removal of selenate in simulated agricultural drainage water by a rice straw bioreactor channel system. J. Environ. Qual. 32(5), 1650−1657. https://doi.org/10.2134/jeq2003.1650.